16th World Conference on Earthquake, 16WCEE 2017
Santiago Chile, January 9th to 13th 2017
Paper N° 1837
Registration Code: S-Z1462880571

NATURAL EARTHQUAKES AS PROXIES FOR INDUCED SEISMIC HAZARD AND RISK: COMPARING PEAK AND CYCLIC INELASTIC RESPONSE

F. De Luca[(1)], S. Kythreotis[(2)], M. J. Werner[(3)], and J.P. Verdon[(4)]

[(1)] *Lecturer, University of Bristol, flavia.deluca@bristol.ac.uk*
[(2)] *Undergraduate Student, University of Bristol, sk12756.2012@my.bristol.ac.uk*
[(3)] *Lecturer, University of Bristol, max.werner@bristol.ac.uk*
[(4)] *Research Fellow, University of Bristol, james.verdon@bristol.ac.uk*

Abstract

Over the last decade, human-induced earthquakes have become more common in the world due to the increased number of operations involving hydraulic fracturing (fracking) of tight hydrocarbon reservoirs, geothermal energy, and wastewater disposal. Although such events rarely exceed magnitude 5, some instances of damage have been noted. Even the smaller events pose risks, as they can cause concern in the local communities, lead to high insurance claims and damage the reputation of operating companies, especially in areas unaccustomed to seismicity.

Some evidence suggests that induced earthquakes cause ground motions that are different from those of natural ones: anthropogenic tremors are shallower and appear to generate smaller stress drops. Because of their shallow depths, induced earthquakes can cause amplitude motions in the immediate vicinity of the epicenter that are larger than those expected from tectonic quakes. Such shaking mainly affects low-rise buildings. There has not been any systematic study, yet, on how the above characteristics of human-induced earthquakes affect the structural responses of buildings and whether patterns of differences exist compared to corresponding natural response that could be used for improved induced seismic risk assessment.

This study presents a framework for assessing the aforementioned differences. First, three datasets of natural, fracking and coal mining earthquake records are collected. Ground motion characteristics are compared. Then, peak and cyclic elastic and inelastic response parameters for different Single-Degree-of-Freedom Systems (SDOFs) are statistically compared through hypothesis testing, setting low magnitude natural earthquakes in the United Kingdom (UK) as the benchmark. Comparison is made in terms of normalized response measure such as the inelastic deformation ratio (C_R) and the equivalent number of cycles (N_e). Results suggest a preliminary conclusion that human-induced events exhibit a trend of higher cyclic normalized inelastic response with respect to natural ones, at least for selected waveforms.

The implications of identifying and quantifying such differences in structural response between natural and human-induced earthquakes is relevant to design and retrofit of buildings in non-seismic prone areas, as well as to damage predictions for insurance purposes. Conclusions may be of interest to UK regulatory bodies in the preparation of recommendation documents for areas potentially affected by human-induced earthquakes.

Keywords: fracking; mining; inelastic deformation ratio; equivalent number of cycles; hypothesis tests.

1. Introduction

It is now widely accepted that the number of human-induced earthquakes has increased in recent years, and especially in the last decade [1]; [2]. In the central United States, more than 1,000 earthquakes occurred in 2015 alone, with magnitude greater than 3, compared to an annual average of 24 between 1973 and 2008 [3]. This exponential increase in events is attributed to the increased rate of human activities that are prone to induce seismicity, such as wastewater disposal and hydraulic fracturing.

Recent studies by [4] and [5] either conclude, or employ the assumption, respectively, that Ground Motion Prediction Equations (GMPEs) derived from natural and human-induced earthquakes are comparable for similar magnitudes and hypocentral distances (GMPEs for atectonic earthquakes are sometimes specifically calibrated for shallower and smaller earthquakes). The equivalence of the structural response to naturally occurring and human-induced events, however, has not yet been assessed. This is important because the structural response is not solely a function of the parameters that are typically contained in GMPEs, such as Peak-Ground-Accelereation (PGA) etc., and could therefore be different for tectonic and atectonic quakes. The structural response has direct implications for seismic design, insurance estimates, and government regulation bodies. This study is mainly focused on the investigation of such equivalence, with specific reference to the potential application of such results to the UK.

Current literature is reviewed to introduce the different causes of induced seismicity and to look into differences in characteristics relative to natural events (section 2). A compiled dataset of past earthquake ground motions is presented (section 3), consisting of three sets – namely UK natural, and worldwide induced and mining-related earthquakes (United States and Canada). Prior to any structural analysis, various ground motion parameters are computed in order to better understand and contextualise differences between the three datasets. We analyze the elastic and inelastic response for two distinct Single-Degree-of-Freedom (SDOF) systems for the horizontal components of each station record. We compute peak and cyclic response parameters for the inelastic SDOFs, in the form of the inelastic displacement ratio (C_R) and equivalent number of cycles (N_e), respectively, for two distinct strength reduction factors (section 4). Finally, we employ hypothesis testing to compare the three datasets, using the natural set as a benchmark, for both peak and cyclic response parameters (section 5). Results show evidence of differences in the inelastic displacement ratios mainly between the natural and induced sets at low structural periods. Greater variation is observed in equivalent number of cycles for both mining and induced sets compared to the natural, over the entire range of periods (section 6). This suggests a higher possible sensitivity of cyclic response parameters to the different motion characteristics between natural and induced/mining events.

2. Human-Induced Earthquakes

Human-induced earthquakes are produced by a variety of different activities – mainly fracking, wastewater disposal, geothermal energy production, carbon capture and storage and coal mining. The largest injection-induced event, which occurred in Oklahoma in 2011, had a magnitude (M_w) of 5.6 and was triggered by wastewater disposal. This event destroyed 14 houses and injured 2 people. Considering that the Local Magnitude (M_L) threshold for structural damage is often assumed to be 4 ([6]; [7]), induced events are capable of causing severe disruption to the built environment and can result in loss of human lives. The most common activities causing induced seismicity are described herein.

Fracking is the process by which controlled injection of water, sand and chemicals under pressure directed at rocks leads to tensile fractures and increases the permeability of, mainly, tight shale formations to provide conduits for oil and gas to flow through ([1]; [6]; [8]). In the UK, two fracking induced earthquakes have been identified so far, at Blackpool in 2011, with M_w 2.3 and 1.5, respectively. While not strong enough to cause structural damage, the events raised alarm towards the fracking activities from residents. Subsidence above conventional oil and gas fields can also cause seismicity. The 2012 magnitude 3.6 event in the Groningen field of the Netherlands, in a region regarded as aseismic before gas production began in 1986, resulted in 30,000 individual damage claims directed towards the operating company [9], demonstrating the economic impact that even small induced earthquakes can have in a region unaccustomed to seismicity. Another example is the M_L 3.4 earthquake at the Basel geothermal site in Switzerland in 2006 [10].

Wastewater disposal is regarded as the process most capable of inducing high magnitude human-related earthquakes (see the Oklahoma case) [11]. In this category, it is included the injection of saline water into underground wells, examples of which occurred at the Paradox Valley, Colorado and the KTB drilling site in Germany ([12]; [13]), as well as fluid injection for enhanced oil recovery.

Mining activities are among the most widely studied causes of induced seismicity. There are generally three ways that mining can produce earthquakes. One is when mine workings collapse, causing ground motions ranging between Mw 1.6 to 5.6 [14]. The second way is a direct result of the excavation of material, which causes a reduction in normal stress in the soil layers underneath, and consequently a reduction in the shear capacity of the rock that can fail as a result. The third way is due to rock blasts, which are recognized by waveforms with very acute initial spikes. Unlike induced seismicity, with mining it is possible to control where, when and how big the blasts will be.

The driving mechanism that causes induced earthquakes from fracking, wastewater disposal is well documented and it has to do with the shear capacity of the fault given by the Mohr-Coulomb formula, where μ is the friction coefficient, σ_v the total vertical stress, P the pore water pressure, and c the cohesion of the soil:

$$\tau_{crit} = \mu \cdot (\sigma_v - P) + c \quad (1)$$

Fault rupture occurs when the applied shear stress exceeds the shear capacity of the fault (τ_{crit}). This can be caused by increasing the shear stress, reducing the normal stress or increasing pore water pressure. An increase in pore pressure is the main reason why fracking and wastewater disposal activities induce microseismic events and potential earthquakes. As mentioned above, mining can result in reduced normal stress and failure due to solid or fluid extraction. Fluid extraction from reservoirs will alter both then normal and shear stresses in the surrounding rocks, potentially causing seismicity [15]. Water extraction from an aquifer is believed to have caused the magnitude 5.1 Lorca earthquake in Spain in 2011 that killed 9 people and caused widespread damage to the non-seismically designed buildings ([1]; [16]).

Induced earthquakes have several distinct features that are important when considering their effects on structural response. They usually nucleate at a focal depth of less than 5km ([5]; [17]) compared to a range of 3-20km depth for shallow crustal earthquakes [19]. In intraplate areas, like the UK, for a natural event of magnitude greater than 4 or 5 - enough to cause structural damage - a fault rupture of several kilometres is required and it usually only occurs at depths greater than 10km [6]. According to Hough ([17]), “stress drops of injection-induced earthquakes are systematically lower than tectonic earthquakes by an estimated factor of 2-10”. A possible hypothesis is that for an induced event, not as much stress is allowed to accumulate as when the fault ruptures naturally. As such, shaking intensity is lower and the effects less pronounced at moderate to large distances from the epicentre. At the immediate epicentral region, within a radius of 10km, the shallow depth does enough to offset the lower stress drop and cause similar or even greater shaking compared to a tectonic earthquake occurrence ([17]). As a result, ground motions can be of large amplitude and structural damage more manifest [5]. Bommer et al ([18]) suggest that due to the shallow nature of induced earthquakes, wave propagation from the rupture will be more strongly dependent on soil type and homogeneity of the upper portion of tectonic crust, resulting in greater regional differences in earthquake characteristics. This is shown by Bourne et al ([19]) who concluded that a GMPE developed using earthquakes from all over the Netherlands was not applicable to the particular case of the Groningen Field due to its distinct upper crust conditions.

In terms of structural response, shallow earthquakes are known to affect structures with lower structural periods largely, because of their higher frequency content. This agrees with the Type 2 ($M_L < 5.5$ events) elastic response horizontal spectra in Eurocode 8 (EC8), which shows a higher peak spectral acceleration at structural periods less than 0.4 sec with respect to the Type 1 shape [21].

3. Dataset development

Three datasets were compiled based on earthquake induction cause, namely natural, coal mining, and injection-induced. Since the conclusions of this paper aim to be especially relevant to the UK, past natural, tectonic events were selected from there. Coal mining and injection-induced earthquake waveforms were retrieved from the UK

when possible and supplemented with events from the US and Canada due to limited availability. Table 1 below summarises the three datasets compiled and Fig.1 illustrates the event locations and magnitudes. Both table and figure refer to the processed data. Data was obtained through interrogation of the global seismic database network IRIS (see data acknowledgements). For IRIS interrogation, earthquake event location, time, depth and magnitude were all necessary parameters to be identified for every event, prior to interrogation. This was made possible through existing lists of events in the literature and online ([22]-[29]).

Table 1 – Summary of the waveforms selected for each subset

	Number of Waveforms								
Region\Type	**Natural**			**Coal Mining**			**Injection-Induced**[1]		
	Events	**Components**		**Events**	**Components**		**Events**	**Components**	
		Horizontal	**Vertical**		**Horizontal**	**Vertical**		**Horizontal**	**Vertical**
UK	20	44	23	1	2	1	-	-	-
US	-	-	-	-	-	-	6	26	12
Canada	-	-	-	16	44	23	-	-	-
Total	20	44	23	17	46	24	6	26	12

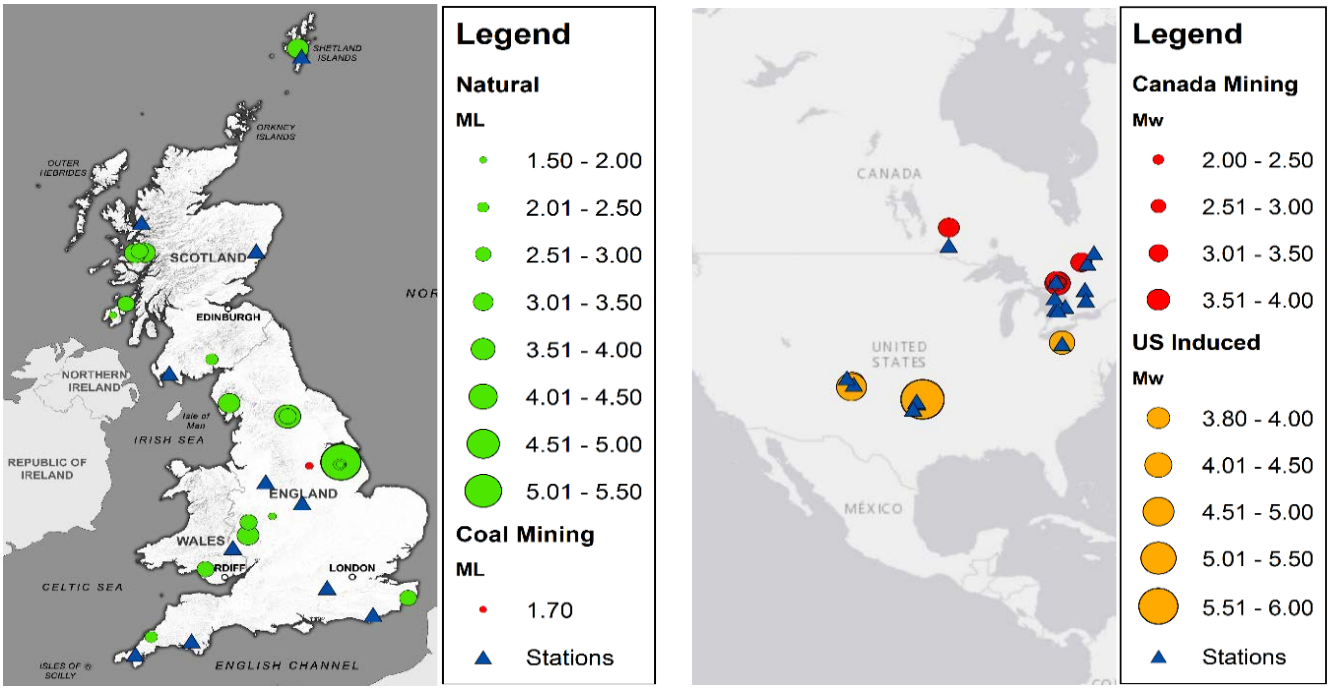

(a) (b)

Fig. 1 – Map showing location and magnitude of earthquakes and stations used to develop the ground motion dataset (a) for the UK, and (b) for US and Canadian earthquakes.

A preliminary processing of the waveforms is made herein. To make the three datasets potentially useful from a vulnerability point of view; we set up a lower limit on Peak Ground Acceleration (PGA) and an upper limit on epicentral distance (R_{epi}), see Eq. (2). Events and stations presented in Fig.1 have at least one of their three waveform components passing the filtering criteria in Eq. (2).

$$PGA \geq 0.1\, cm/s^2 \quad \& \quad R_{epi} \leq 300\, km \tag{2}$$

[1] Induced events here are those caused by fluid injection.

The selection of the criteria is a balance between a reasonable limit and the necessity to have a sufficient number of records to carry out preliminary observations on potential response differences between the three sets of records. The main problem with waveform availability for induced events was the unavailability of seismographs covering the event at the time and location of occurrence. For example, although Wilson et al. ([26]) provided an extensive list of UK past earthquakes, the IRIS networks for the UK had very limited data available prior to 2003, inhibiting waveform retrieval for these earthquakes. Evidence for the difficulty in obtaining suitable waveforms for this study is the fact that out of the 77 induced events for which data was obtained for, only six made it past the filters.

The value of PGA selected is significantly low as threshold for structural and non-structural damage, and R_{epi} is by far higher than the typical limit of interest for induced seismicity (e.g., typically within 50 km). As an example, the recent bespoke GMPE by Atkinson [5] considers data recorded within 40km. Regarding PGA threshold, EC8 defines the minimum PGA for seismic design as 0.04g [30], corresponding this value to 10% probability of exceedance in 50 years. Minor plaster cracking can occur at PGA values as low as 0.08 m/s^2 based on a formulation made with Californian earthquakes ([31]; [32]). As already mentioned, induced seismicity is common in areas unaccustomed to seismicity, where residents easily feel tremors equivalent to modified Mercalli intensity (MMI) between grade one and two. Such values can correspond to quite variable value of PGA up to lower bound limit of 0.1cm/s^2 (see [33] for details). Based on the above considerations, criteria in Eq. (2) are significantly relaxed, but they allow a sufficient number of waveforms to pass aimed at showing the methodological approach discussed herein.

According to Douglas & Boore ([34]), low-frequency noise (<1 Hz) can have a dramatic impact on Intensity Measures (IMs), such as spectral response ordinates, and their removal is standard procedure. Additionally, the same source supports that "records with poor high-frequency signal-to-noise ratios are likely to be those with low amplitudes, i.e. from small earthquakes and/or long distances", which applies to the waveforms retrieved in this study. In this study, we use a linear baseline correction and a bandpass Butterworth filter of 4th order at cut-off frequencies of 0.1 and 25 Hz, which approximately corresponds to the filtering configuration usually employed by strong-motion databases to obtain corrected accelerogram records (e.g., [35]). Ideally, filtering has to be carried out at unique bandpass corner frequencies for every waveform, identified using a Fourier amplitude spectrum as the frequencies containing low signal-to-noise ratio ([36]). Such filtering can be crucial for induced records considered, as emphasized in [20] and the best low cutoff frequency can be higher than 0.1 Hz. On the other hand, at this preliminary stage of this methodological study, only normalized engineering demand parameters (EDPs) are used (see section 4) and periods of the SDOFs considered are up to 1s making results not affected by the low cutoff frequency of 0.1 Hz.

An essential part of the dataset's development is to assess whether natural, induced and mining events had adequate overlap in terms of ground motion characteristics. This is important as structural response comparison depends largely on it. In order for subsequent conclusions to be useful and meaningful, an acceptable degree of overlap is deemed necessary. In Fig. 2, the plot of M_W versus Hypocentral distance for the events in the three datasets is shown.

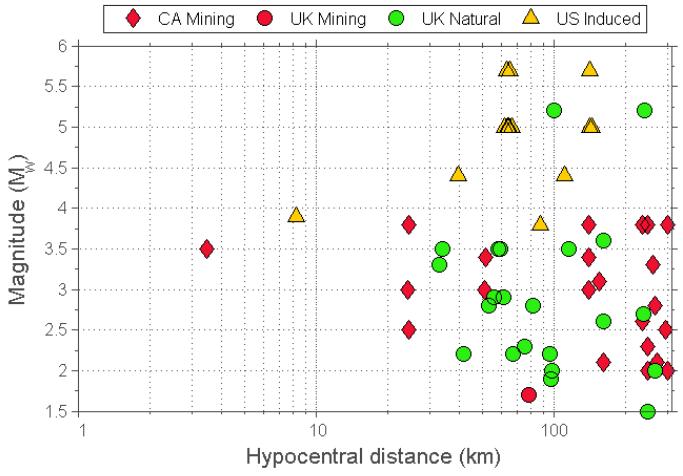

Figure 2 - Earthquake (a) Magnitude of the three datasets of events in shown in Table 1

Five ground motion parameters are considered: PGA, Peak Ground Velocity (PGV), Arias Intensity (I_A) and 5-95% significant duration (S_D). In Fig.3, all these parameters are shown for the three datasets.

Fig. 3 shows a sufficient overlap between the datasets, especially between UK natural and coal mining events across all the parameters plotted. US induced events are those with higher IMs. A suggestion for further work would be to supplement the database to better bridge this gap, perhaps by using natural earthquakes from other national databases, as well as retrieving more induced waveforms when publicly available.

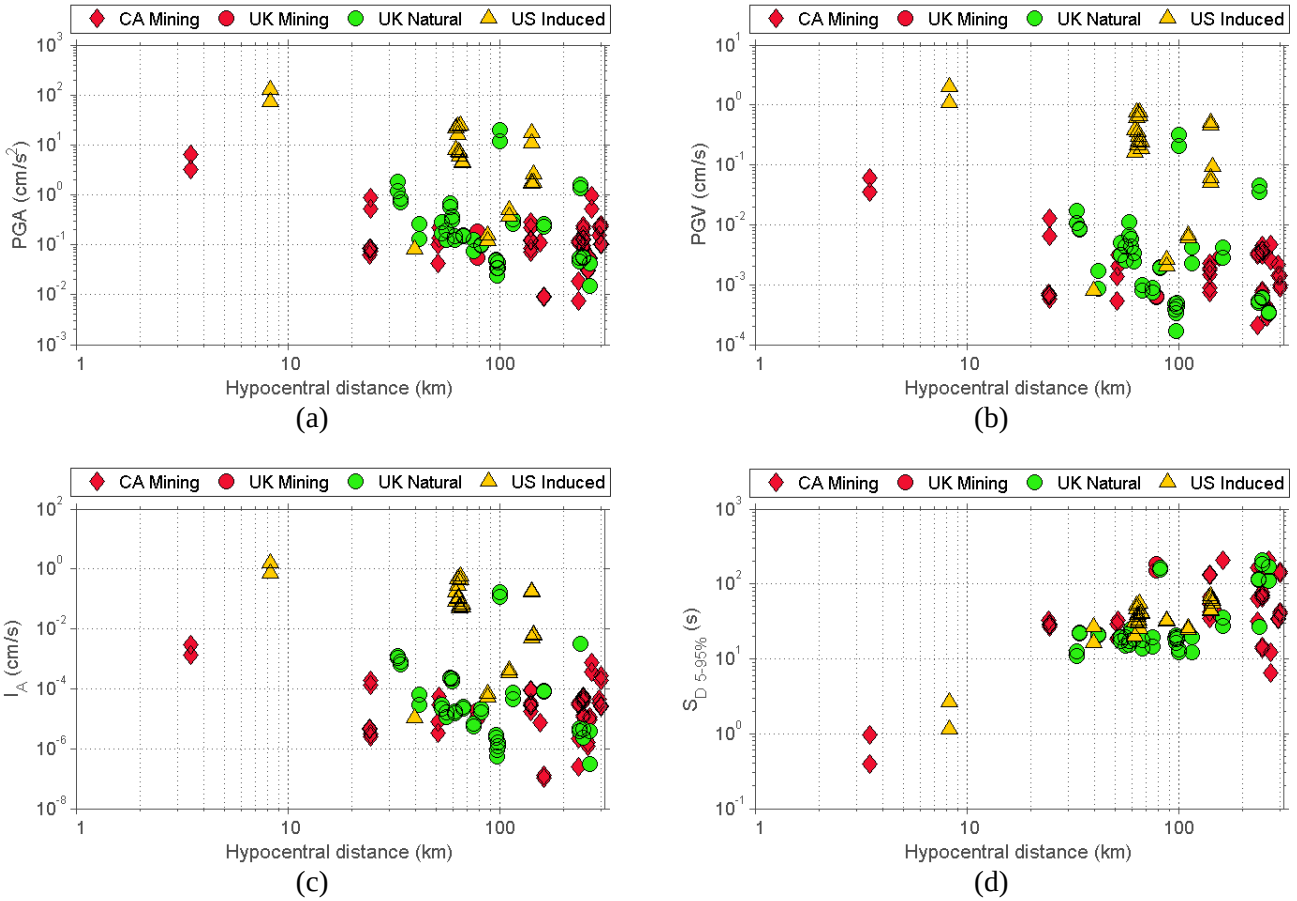

Figure 3 - (a) PGA, (b) PGV, (c) I_A and (d) S_D (5-95%) for both horizontal components of the corrected waveforms.

5. Structural Response

In order to better understand the three datasets and to identify differences in their structural responses, three SDOF systems with different strength and stiffness characteristics were selected. For each SDOF system shown in Fig.4, the peak response was evaluated. For the two inelastic SDOFs, both peak and cyclic response parameters were computed for later comparison using hypothesis testing. The first SDOF is a linear-elastic system; it is employed to determine the peak elastic displacement (Δ_{el}) and Pseudo Spectral Acceleration (PSA). In Fig.4b and 4c, the two inelastic SDOFs are represented: the first is an Elastic-Plastic with Hardening and a kinematic hysteresis rule (EPH), the second is an Elastic-Strength/Stiffness-Degrading (ESD) with a piching hysteresis [37]. For the EPH system, post-yield stiffness is assumed to be 5% of the elastic value, whereas in the ESD post-yield stiffness was -10% of the elastic value. In addition, the residual strength (F_{res}) is taken as zero for the ESD system. These two SDOFs were used in the inelastic analysis to compute both peak and cyclic response parameters, in the form of the inelastic deformation ratio (C_R) and equivalent number of cycles (N_e), respectively. The structural periods used are 0.03, 0.05, 0.10, 0.20, 0.30, 0.50, 1 seconds, and the damping ratio

is set at 5% for both elastic and inelastic analyses. Such period values represent reasonably well the one- or two-storey masonry structures typical of rural areas in the UK, and they are not affected by the preliminary waveform correction made in this study.

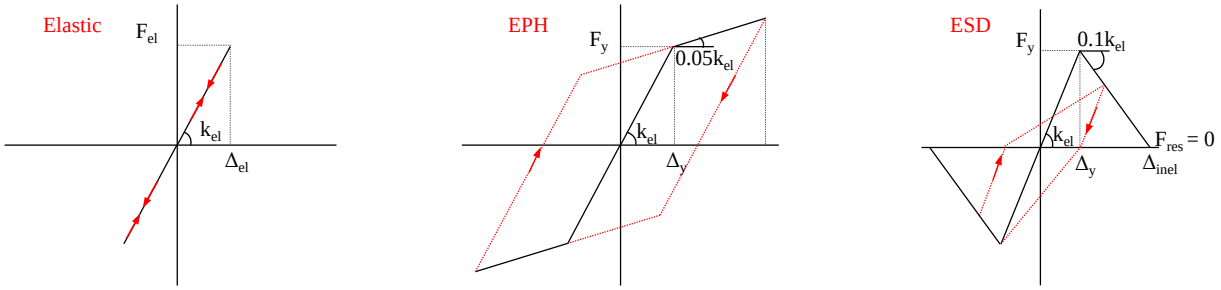

(a) (b) (c)

Figure 4 - SDOF systems analysed (a) Linear Elastic, (b) EPH (c) ESD [adapted from [38]].

Elastic spectra were employed for the evaluation of Δ_{el} for the computation of C_R. Fig.5 presents the results of the elastic analysis for each of the three datasets. It can be observed that the spectral envelope for the natural and mining categories is similar, tying up with the observations of sufficient overlap evidenced in Fig.3. Conversely, the spectral envelope for the injection-induced dataset is evidently shifted to higher values, with a mean curve as much as 10 times greater than the other two datasets. This is the reason why using C_R, instead of the peak inelastic displacement (Δ_{inel}) employed in other studies (e.g. [38]), is the only feasible approach to draw conclusions on peak response. In fact, C_R has been proven to be less susceptible to differences in the aforementioned characteristics, as well as soil conditions, between the datasets ([39]-[41]).

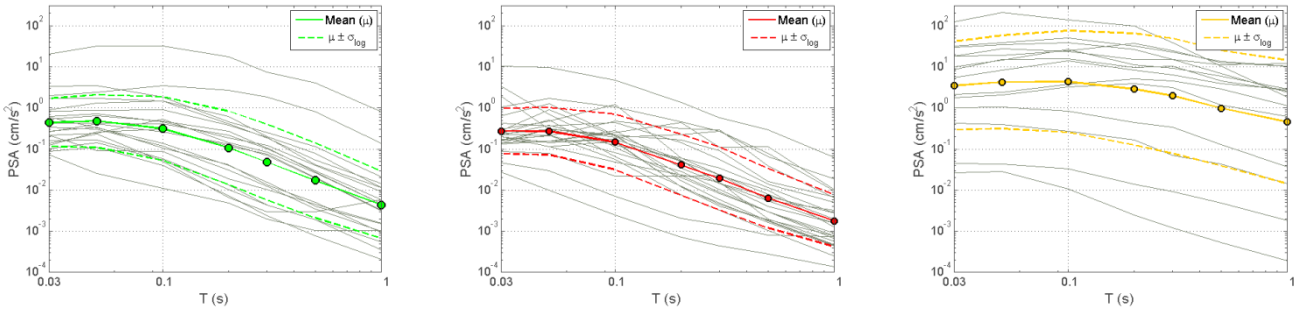

(a) (b) (c)

Figure 5 - Geometric mean of the two horizontal components of each waveform in grey and their median ± logarithmic standard deviation (σ_{log}) in green, red and orange for (a) natural, (b) mining and (c) induced events.

For inelastic analysis, the choice of yield strength (F_y) for the EPH and ESD systems has to be made. Common design practice suggests the application of a strength reduction factor (R) to reduce the peak elastic force (F_{el} in Fig.4a) as given by Eq. (3). Multiple R values ranging from 1.5 to 3 in intervals of 0.5 were analysed, but only those of 1.5 and 3 will be presented for the sake of brevity; R values signify low to mid ductile structures with R increasing. Justification for the lower bound of 1.5 is that the limiting value for non-dissipative structures in EC8 is a behaviour factor (q) of 1.5 for elastic design, to account for implicit overstrengths in design; q being similar to R in this case [21]. The R upper bound value of 3 is justified by the fact that this is the allowable upper bound for the behaviour factor of existing buildings in many codes (e.g., [42]); existing buildings reasonably match the class of non-seismically designed structures that are likely to experience any damage from induced seismicity.

$$F_y = F_{el} / R \tag{3}$$

As discussed in Bazurro, et al. ([43]), two approaches can be adopted in applying R to determine F_y – the *constant-R* and *constant-strength* approaches – that can yield different conclusions. In the first approach, F_y is obtained by applying R to the F_{el} values of each waveform individually, thus forcing yielding in every case. The disadvantage of such an approach is that the value of F_y obtained is a record-related variable, when F_y is typically a structure-related characteristic. In the second approach, F_y is obtained by applying R to the median F_{el} value of the pool of records in question. The problem with this approach is that variability within the dataset due to outliers (evident in Fig.5) can greatly affect F_y, and cause some SDOF systems to yield and many others not to, when subjected to the ground motions in the dataset. Given these considerations, the constant-R approach is adopted. The geometric mean of the two horizontal components for each record is used to compute C_R and the hysteretic energy-based cyclic response parameter N_e (i.e., the equivalent number of cycles), see Eq.(4) and (5). E_H is the cumulative hysteretic energy, evaluated as the sum of the areas of all hysteretic cycles (not considering the contribution of viscous damping) and normalised by the area under the backbone curve between peak inelastic displacement Δ_{inel} and yield displacement Δ_y for the largest cycle ($A_{plastic}$), see [44] for details.

$$C_R = \Delta_{inel} / \Delta_{el} \tag{4}$$

$$N_e = \left(E_H / A_{plastic} \right) + 1 \tag{5}$$

The results of the inelastic analysis are shown for R values of 1.5 and 3 in Fig.6, for both the EPH and ESD SDOF systems. In order to compare and validate the results, curves were plotted for the C_R characterisation equations proposed by Ruiz-Garcia & Miranda ([40]) and Chopra & Chintanapakdee ([41]). The Ruiz-Garcia and Miranda curves (R-M) are plotted for soil conditions B and D corresponding to rock with Vs 760-1525 m/s and stiff soil with Vs 170-360 m/s, respectively. The equation proposed by Chopra & Chintanapakdee is independent of soil conditions. It is worth noting that the two proposed equations are based on bilinear systems, similar to EPH. Also, the effect of post-yield stiffness is taken into consideration in the relation proposed by Chopra & Chintanapakdee, but not that of Ruiz-Garcia and Miranda.

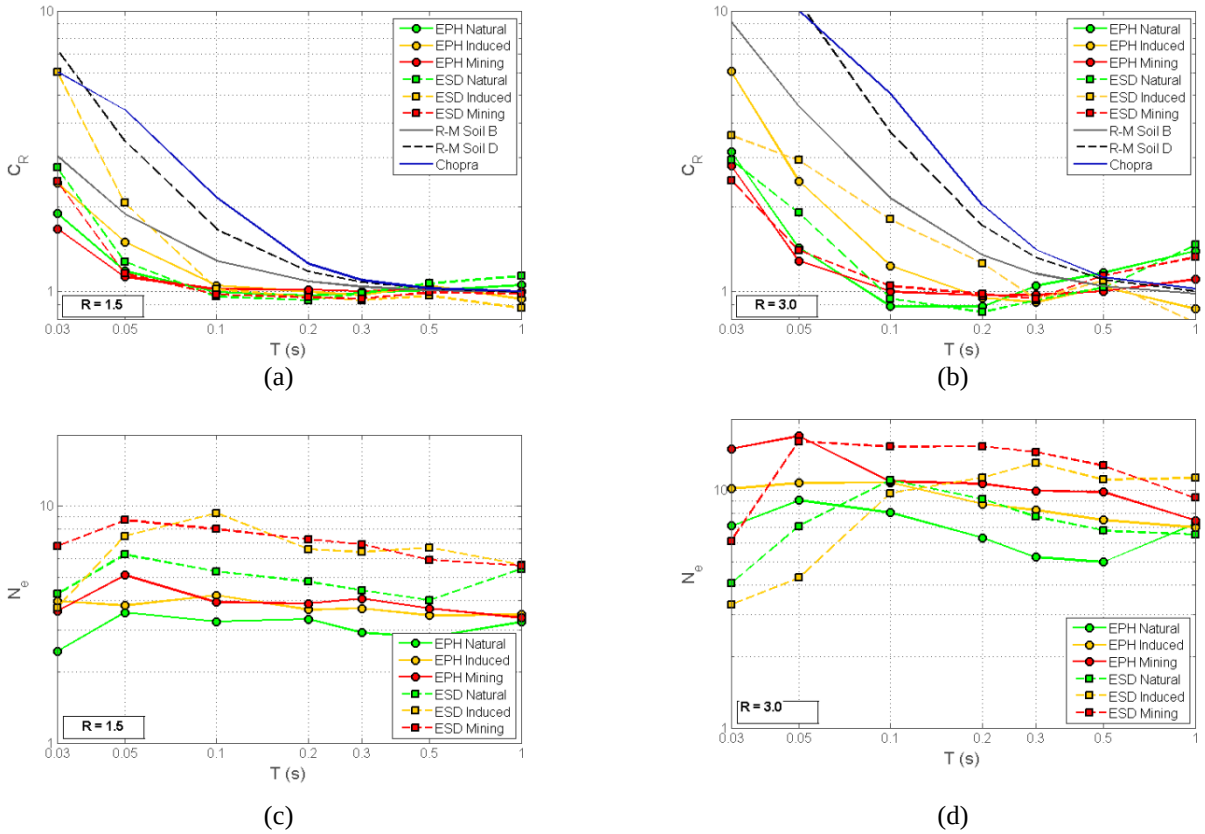

Figure 6 - C_R results for EPH and ESD systems with added curves by Ruiz-Miranda ([40]) and by Chopra & Chintanapakdee ([41]) for (a) R=1.5, (b) R=3; and N_e results for (c) R=1.5 and (d) R=3.

As expected [41], the results of C_R show large sensitivity to F_y (based on R) in the acceleration-sensitive part of the spectrum (T<0.5s), while at higher periods the differences between the datasets become less marked and C_R gets closer to 1, following the equal displacement rule. In Fig.6, the two SDOF systems exhibit some variation in their structural responses. In terms of C_R, the ESD system shows an increase compared to the EPH for T<0.1s, and T<0.3s at R=3 for induced events. A significant increase in the N_e values is observed in the ESD system compared to the EPH throughout the period spectrum for R=1.5. The same holds true for R=3, except in the lower part of the period spectrum for which a decreasing trend in N_e is evident; the period range of such decrease varies for each dataset. It is evident that structural response results are significantly affected by the SDOF system chosen, as well as by the choice of R made. It is therefore fundamental that a correct characterisation of real structures is made.

6. Hypothesis testing

In order to assess whether the earthquake cause (natural, injection-induced, or mining) can influence the structural response from the resulting earthquake, we quantitatively assessed the similarity of the results from the three datasets through hypothesis testing. The null hypothesis tested is whether the median of geometric means for the mining and injection-induced horizontal components of the waveforms can be considered equal to the median of geometric means of the natural dataset. To do so, a two-tailed Aspin-Welch test is carried out, because of its suitable assumption that the variances of the populations tested do not have to be equal – which would be very unlikely in this case (see Fig.5). The assumption of lognormally distributed datasets for all the datasets and for both C_R and N_e is made. The test is conducted at a 95% confidence level for C_R and N_e, for both the EPH and ESD systems. Results for EPH and ESD SDOFs are shown in Fig.7. Results in Fig. 7 show that, in terms of C_R, there is good agreement between the mining and natural datasets over the entire period spectrum, for both R values, with only 1 p-value being less than the alpha (α) value of 0.05. Rejections are more evident for the injection-induced dataset, the expected spectral range of structures in non-seismically designed areas and, to some extent, in the velocity-sensitive part of the spectrum (0.5<T<1s). Increasing the nonlinearity (i.e., R=3, mildly inelastic response) leads to increased rejections. In terms of N_e, more rejections are evident in a general sense, suggesting a higher possible sensitivity of cyclic response due to differences in earthquake characteristics. Roughly the same rejections are shown in both R cases, the p-values for mining are in the rejection area for the acceleration-sensitive region (T<0.5s), in both figures of N_e.

7. Conclusions and further developments

Human-induced seismicity is becoming increasingly relevant in the world today, and many recent studies have primarily focused on the causes of such seismicity. Herein, a methodological approach is discussed to check whether peak and cyclic structural response can be considered different between natural and human-induced events. Three datasets of natural, coal mining and injection-induced events are compiled and compared in terms of ground motion characteristics. The induced waveforms in consideration have an upper bound presence in the intensity measures computed, compared to a better match between the mining and natural datasets. This is also reflected in the elastic response spectra, in which the induced dataset shows a marked difference with respect to the others. The three datasets are used to evaluate the inelastic response of two different SDOF systems – EPH and ESD – with different stiffness and strength characteristics, at multiple yield strengths. Conclusions are drawn based on hypothesis tests that quantitatively assess the difference in median inelastic deformation ratio and equivalent number of cycles computed for each waveform in each dataset, using the natural set as the benchmark. Notwithstanding the differences between the datasets in terms of intensity measures, both parameters selected to compare peak and cyclic inelastic responses are of a non-dimensional nature allowing a consistent comparison and preliminary conclusions. The observations drawn are that there is good agreement between the natural and mining datasets in terms of C_R, but less between natural and induced, especially for structural periods lower than one second. Result trends are similar for both SDOF systems. The cyclic response parameter, N_e, appears to have a higher sensitivity to differences between natural and human-induced events,

with a larger number of rejections of the equal means hypothesis at 95% confidence level, for both mining and induced events compared to the natural dataset.

The aim of this study is to draw a methodological approach for the comparison of natural and human-induced earthquakes in terms of structural response. A framework for this comparison is presented, but in order to make the conclusions reliable a larger and richer database of natural, induced and mining waveforms needs to be developed. This will help to achieve better overlap in terms of ground motion characteristics and will lead to a comparison of like-for-like datasets. It will also facilitate comparison with GMPEs (impossible in this study because of limited data at low distances in the dataset).

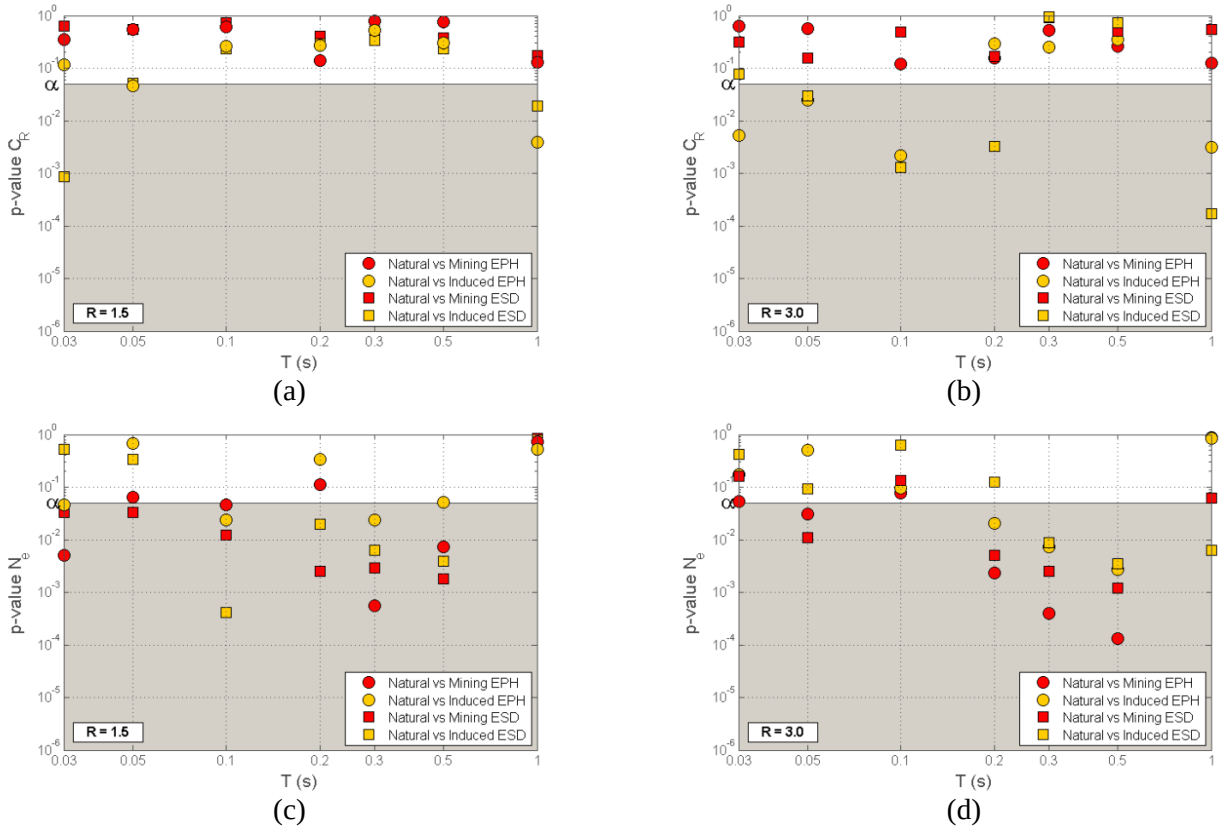

Figure 7 - Hypothesis test results for C_R in case of (a) R=1.5 and (b) R=3, and N_e in case of (c) R=1.5 and (d) R=3 for the EPH (circle markers) and ESD (square markers) systems

Data Acknowledgements

The facilities of IRIS Data Services, and specifically the IRIS Data Management Centre, were used for access to waveforms, related metadata, and/or derived products used in this study. IRIS Data Services are funded through the Seismological Facilities for the Advancement of Geoscience and EarthScope (SAGE) Proposal of the National Science Foundation under Cooperative Agreement EAR-1261681. This is available at http://www.iris.edu/hq/ (accessed 06/02/16).

References

[1] Ellsworth W. L. (2013). Injection-Induced Earthquakes. Science 341(6142).

[2] USGS (2015). USGS Earthquake Hazards Program: Induced Earthquakes, [online]. See http://eathquake.usgs.gov/research/induced/ (accessed 12/06/2015)

[3] Bloomberg News (2016). Here's the U.S. Earthquake Forecast, Now Including the Quakes We Cause, [online]. See http://www.bloomberg.com/news/articles/2016-03-28/u-s-quake-forecast-includes-human-induced-temblors-for-first-time (accessed 03/04/2016)

[4] Douglas, J., Edwards, B., Convertito, V., Sharma, N., Tramelli, A., Kraaijpoel, D., . . . Troise, C. (2013). Predicting Ground Motion from Induced Earthquakes. Bulletin of the Seismological Society of America 103(3): 1875–1897.

[5] Atkinson, G. (2015). Ground-Motion Prediction Equation for Small-to-Moderate Events at Short Hypocentral Distances, with Application to Induced-Seismicity Hazards. Bulletin of the Seismological Society of America 105(2A): 981–992.

[6] Green, C., Styles, P., and Baptie, B. (2012). Preese Hall Shale Gas Fracturing: Review and Recommendations for Induced Seismic Mitigation, available from: https://www.gov.uk (accessed 10/04/2016)

[7] ICHESE (2014). Report on the Hydrocarbon Exploration and Seismicity in Emilia Region. International Commission on Hydrocarbon Exploration and Seismicity in the Emilia Region, available from: http://docplayer.net/ (accessed 10/04/2016).

[8] BBC News (2013). What is fracking and why is it controversial?, [online]. See http://www.bbc.co.uk/news/uk-14432401 (accessed 26/10/2015)

[9] Dost, B., Kraaijpoel, D., van Eck, T., Caccavale, M., and Bilt, d. (2015). Hydrocarbon Induced Seismicity in Northern Netherlands. In SECED Conference: Earthquake Risk and Engineering towards a Resilient World: Cambridge, UK 9-10 July 2015.

[10] Goertz-Allmann, B. P., Goertz, A., & Wiemer, S. (2011). Stress drop variations of induced earthquakes at the Basel geothermal site. Geophysical Research Letters, 38(9).

[11] McGarr, A. (2014). Maximum magnitude earthquakes induced by fluid injection. Journal of Geophysical Research: Solid Earth 119(2): 1008-101. http://dx.doi.org/10.1002/2013JB010597

[12] Ake, J., Mahrer, K., O'Connell, D., and Block, L. (2005). Deep-Injection and Closely Monitored Induced Seismicity at Paradox Valley, Colorado. Bulletin of the Seismological Society of America 95(2): 664–683.

[13] Zoback, M., and Harjes, H.-P. (1997). Injection-induced earthquakes and crustal stress at 9 km depth at the KTB deep drilling site, Germany. Journal of Geophysical Research 102: 18,477-18,491.

[14] Davies, R., Foulger, G., Bindley, A., and Styles, P. (2013). Induced seismicity and hydraulic fracturing for the recovery of hydrocarbons. Marine and Petroleum Geology 45(2013): 171-185.

[15] Segall P., Earthquakes triggered by fluid extraction. Geology 17, 942-946.

[16] De Luca, F., Verderame, G., Gomez-Martinez, F., and Perez-Garcia, A. (2014). The structural role played by masonry infills on RC building performances after the 2011 Lorca, Spain, earthquake. Bulletin of Earthquake Engineering 12(5): 1999-2026.

[17] Hough, S. E. (2014). Shaking from Injection-Induced Earthquakes. Bulletin of the Seismological Society of America 104(5).

[18] McGarr, A., and Fletcher, J. (2005). Development of Ground-Motion Prediction Equations Relevant to Shallow Mining–Induced Seismicity in the Trail Mountain Area, Emery County, Utah. Bulletin of the Seismological Society of America 95(1): 31–47.

[19] Bommer, J., Dost, B., Edwards, B., Stafford, P., van Elk, J., Doornhof, D., and Ntinalexis, M. (2016). Developing an Application-Specific Ground-Motion Model for Induced Seismicity. Bulletin of the Seismological Society of America 106(1).

[20] Bourne, S., Oates, S., Bommer, J., Dost, B., van Elk, J., and Doornhof, D. (2015). A Monte Carlo Method for Probabilistic Hazard Assessment of Induced Seismicity due to Conventional Natural Gas Production. Bulletin of the Seismological Society of America 105(3): 1721–1738.

[21] Comité Européen de Normaliation (CEN) (2004). European Standard EN 1998-1. Eurocode 8: Design of structures for earthquake resistance - Part 1: General rules, seismic actions and rules for buildings, pp. 17, 25. Comité Européen de Normaliation, Brussels, Belgium.

[22] Healy, J., Rubey, W., Griggs, D., and Raleigh, C. (1968). The Denver Earthquakes: Disposal of waste fluids by injection into a deep well triggered earthquakes near Denver, Colorado. Science 161(3848)

[23] Kim, W.-Y. (2013). Induced seismicity associated with fluid injection into a deep well. Journal of Geophysical Research: Solid Earth 118(7): 3506–3518.

[24] Seeber, L., Armbruster, J., and Kim, W.-Y. (2004). A Fluid-Injection-Triggered Earthquake Sequence in Ashtabula, Ohio: Implications for Seismogenesis in Stable Continental Regions. Bulletin of the Seismological Society of America 94(1): 76–87.

[25] Rubinstein, J., Ellsworth, W., McGarr, A., and Benz, H. (2014). The 2001–Present Induced Earthquake Sequence in the Raton Basin of Northern New Mexico and Southern Colorado. Bulletin of the Seismological Society of America 104(5): 2162–2181.

[26] USGS (2012). USGS Earthquake Hazards Program: Mining-Induced Events in the Earthquake Catalogs of the USGS/NEIC, [online]. See http://earthquake.usgs.gov/earthquakes/eqarchives/mineblast/induced_pde.php (accessed 06/02/2016)

[27] Wilson, M., Davies, R., Foulger, G., Julian, B., Styles, P., Gluyas, J., and Almond, S. (2015). Anthropogenic earthquakes in the UK: A national baseline prior to shale exploitation. Marine and Petroleum Geology 68(A): 1-17.

[28] Petersen, M.D., Mueller, C.S., Moschetti, M.P., Hoover, S.M., Rubinstein, J.L., Llenos, A.L., Michael, A.J., Ellsworth, W.L., McGarr, A.F., Holland, A.A., and Anderson, J.G. (2015). Incorporating induced seismicity in the 2014 United States National Seismic Hazard Model - Results of 2014 workshop and sensitivity studies: U.S. Geological Survey Open-File Report 2015–1070.

[29] Natural Resources Canada (2016). Earthquakes Canada, GSC, Earthquake Search (On-line Bulletin), [online]. See http://earthquakescanada.nrcan.gc.ca/stndon/NEDB-BNDS/bull-eng.php (accessed 06/02/2016)

[30] Carvalho, E. C. (2011). Eurocode 8 Background and Applications: Overview of Eurocode 8, available from: http://eurocodes.jrc.ec.europa.eu/doc/WS_335/S1_EC8-Lisbon_E%20CARVALHO.pdf (accessed 10/04/2016)

[31] Wald, D., Quitoriano, V., Heaton, T., and Kanamori, H. (1999). Relationships between Peak Ground Acceleration, Peak Ground Velocity, and Modified Mercalli Intensity in California. Earthquake Spectra 15(3), 557-564.

[32] ABAG Resilience Program (2016). Association of Bay Area Governments: Modified Mercalli Intensity Scale (MMI), [online]. See http://resilience.abag.ca.gov/shaking/mmi/ (accessed 08/04/2016)

[33] Worden, C. B., Gerstenberger, M. C., Rhoades, D. A., & Wald, D. J. (2012). Probabilistic relationships between ground-motion parameters and modified Mercalli intensity in California. Bulletin of the Seismological Society of America, 102(1), 204-221.

[34] Douglas, J., and Boore, D. (2011). High-frequency filtering of strong-motion records. Bulletin of Earthquake Engineering 9(2): 395–409.

[35] European Strong-Motion Database (2008). European Strong-Motion Database, [online]. See http://www.isesd.hi.is/ (accessed 03/02/2016)

[36] Boore, D., and Bommer, J. (2005). Processing of strong-motion accelerograms: needs, options and consequences. Soil Dynamics and Earthquake Engineering 25(2): 93–115.

[37] Ibarra LF, Medina RA, Krawinkler H. Hysteretic models that incorporate strength and stiff-ness deterioration. Earthquake Engineering and Structural Dynamics, 2005; 34: 1489-1511.

[38] Iervolino, I., De Luca, F., and Cosenza, E. (2010). Spectral shape-based assessment of SDOF nonlinear response to real, adjusted and artificial accelerograms. Engineering Structures 32 (9): 2776-2792.

[39] Miranda, E. (2000). Inelastic Displacement Ratios for Structures on Firm Sites. Journal of Structural Engineering ASCE 126(10), 1150-1159.

[40] Ruiz-Garcia, J., and Miranda, E. (2003). Inelastic displacement ratios for evaluation of existing structures. Earthquake Engineering & Structural Dynamics 32(8): 1237–1258.

[41] Chopra, A., and Chintanapakdee, C. (2004). Inelastic Deformation Ratios for Design and Evaluation of Structures: Single-Degree-of-Freedom Bilinear Systems. Journal of Structural Engineering ASCE 130(9): 1309-1319.

[42] C.S.LL.PP (2008). DM 14 Gennaio 2008. Norme tecniche per le costruzioni, 2008. Gazzetta Ufficiale della Repubblica Italiana, 29 (In Italian).

[43] Bazurro, P., Sjoberg, B., and Luco, N. (2004). Post-Elastic Response of Structures to Synthetic Ground Motions. Report: USGS web document, available from: https://geohazards.cr.usgs.gov/ (accessed 10/04/2016).

[44] De Luca, F., Ameri, G., Iervolino, I., Pacor, F., and Bindi, D. (2014). Toward validation of simulated accelerograms via prediction equations for nonlinear SDOF response. Bollettino di Geofisica Teorica ed Applicata 55(1): 85-101.